Electrochimica Acta 269 (2018) 706–713

Contents lists available at ScienceDirect

Electrochimica Acta

journal homepage: www.elsevier.com/locate/electacta

Effect of the electrode potential on the surface composition and crystal structure of $LiMn_2O_4$ in aqueous solutions

Florencia Marchini, Ernesto J. Calvo*, Federico J. Williams

Departamento de Química Inorganica, Analítica y Química Física, Facultad de Ciencias Exactas y Naturales, INQUIMAE-CONICET, Universidad de Buenos Aires, Ciudad Universitaria, Pabellon 2, Buenos Aires, C1428EHA, Argentina

ARTICLE INFO

Article history:
Received 1 November 2017
Received in revised form
18 February 2018
Accepted 20 February 2018
Available online 21 February 2018

Keywords:
Lithium
$LiMn_2O_4$
Extraction
XPS
XRD
Battery electrode

ABSTRACT

Cubic spinel $LiMn_2O_4$ has been studied for the reversible extraction of Li^+ from natural brine after the application of suitable electrode potentials. In this work we report on the insertion/extraction of Li^+ from natural brine of Olaroz salt flat (Jujuy, Argentina) and aqueous LiCl solutions into/from $Li_{1-x}Mn_2O_4$ ($0 < x \leq 1$) to determine changes in the crystal structure and surface composition upon electrochemical polarization. In agreement with the behavior in organic electrolytes, we found that the insertion and extraction of Li^+ proceeds via a two stage process and that the crystal structure undergoes two cubic phase transitions as the lattice is expanded or contracted. Contrary to the behavior in organic solvents, no decomposition layer is formed on the electrode surface and the surface composition can be controlled with the electrode potential. We also found that sodium cations present in natural brine are not inserted into the crystal lattice in the potential window explored, however they are adsorbed on the oxide surface blocking Li^+ adsorption sites and decreasing the rate of Li^+ exchange.

1. Introduction

Since its birth several decades ago, lithium-ion batteries have become the leading energy storage technology in portable electronics and electric vehicles. Different lithium intercalation compounds have been used as cathode materials during its development [1,2]. Cubic spinel lithium manganese oxide ($LiMn_2O_4$) has proven to be one of the most promising cathode materials given its high theoretical energy density compared to other intercalation compounds, low toxicity and low cost [3,4].

$LiMn_2O_4$ is a stable phase with half lithium content in the discharge curve from λ-MnO_2 to $Li_2Mn_2O_4$ [5]. Its crystal structure is an $A[B_2]O_4$ spinel [6] from where lithium ions can be reversibly extracted and inserted either chemically or electrochemically without changing the symmetry of the lattice [7,8]. Nonetheless, a significant capacity fading during cycling has been reported and attributed to several factors. The abundance of Mn(III) within the structure in deeply discharged electrodes could cause a cubic to tetragonal transition phase due to Jahn-Teller distortion, also Mn(III) has a high tendency to dismutate to Mn (IV) and soluble Mn (II) in certain non-aqueous electrolytes [4,9–12]. The loss of crystallinity and lack of homogeneity of the material are also major problems [13].

The behavior of $LiMn_2O_4$ electrodes in aqueous solutions has been studied to a lesser extent than in non-aqueous electrolyte. However, considerable research has been conducted in the recent past when intercalation compounds began to be used for lithium recovery from brines or seawater [14–19]. Lithium ions in aqueous media can be inserted and extracted topotactically into and from the $Li_{1-x}Mn_2O_4$ crystal lattice upon application of an electrode potential with no decomposition of the electrolyte upon cycling [20]. We have earlier provided structural evidence confirming electrochemical Li^+ ion exchange between the solid host and the solution after total charge of $LiMn_2O_4$ and total discharge of $Li_{1-x}Mn_2O_4$ ($x \rightarrow 0$) spinel oxides in aqueous LiCl electrolytes and in natural brine. We have also shown that while the fully charged electrode surface only has Mn(IV) exposed to the aqueous solution, the fully discharged electrode surface contains equal amounts of Mn(IV) and unstable Mn(III). This could make the material more prone to dissolution as no protective surface layer is formed in aqueous solutions. This is in contrast to the behavior in organic electrolytes where a surface stabilization layer of decomposition products is formed at the electrode/electrolyte interface upon cycling [21,22].

Driven by the need of a faster, more efficient and

* Corresponding author.
E-mail address: calvo@qi.fcen.uba.ar (E.J. Calvo).

https://doi.org/10.1016/j.electacta.2018.02.108
0013-4686/

environmentally friendly process for lithium recovery from natural brines, we have developed an electrochemical method to extract LiCl from aqueous solutions in an electrochemical reactor containing a lithium-deficient $Li_{1-x}Mn_2O_4$ cathode, which exhibited high selectivity for lithium ions and stability of the system upon over 200 cycles [23,24]. The electrochemical recovery of lithium from natural brines involves the insertion or extraction of lithium ions to or from $Li_{1-x}Mn_2O_4$ in the presence of large amounts of sodium ions. This opens up the question of the potential Na^+ insertion into the lattice which could form a spinel-type $NaMn_2O_4$ phase known to be thermodynamically unstable [25]. Indeed, spinel-type $Li_{1-x}Mn_2O_4$ ($x \rightarrow 0$) structures serve as a host for Na^+ ions that can be inserted electrochemically in organic-based electrolytes [26]. However, sodium insertion brings along a total structural change (from spinel to a layered phase) which has later been proven to be irreversible [27]. We have previously demonstrated that Na^+ ions are not inserted into $Li_{1-x}Mm_2O_4$ ($x \rightarrow 0$) lattice in the potential window used for Li^+ insertion in aqueous electrolytes [28]. Furthermore, cyclic voltammetry (CV) and chronoamperommetry demonstrated that the presence of Na^+ has a negative effect on the kinetics of lithium intercalation in $Li_{1-x}Mn_2O_4$ electrodes [23,28]. This is in agreement with our recent electrochemical impedance spectroscopy study carried out during lithium insertion and extraction in aqueous media [29].

In the present work, we have studied the surface composition and structural changes of $Li_{1-x}Mn_2O_4$ ($0 < x \leq 1$) electrodes when lithium ions are inserted or extracted in aqueous media as a function of lithium loading (i.e. electrode potential or charge) using electrochemical, X-ray photoelectron spectroscopy (XPS) and X-ray diffraction (XRD) measurements. We have studied the effect of the electrode potential on the surface composition and crystal structure of $Li_{1-x}Mn_2O_4$ electrodes in the absence and presence of sodium ions in solution during the insertion and extraction of lithium ions.

2. Experimental

Natural brine from Olaroz, Jujuy (Argentina) has been employed with a chemical composition analyzed by ICP: Na^+ 115.600 ppm (5 M NaCl), K^+ 10.780 ppm (0.28 M KCl), Mg^{2+} 2.618 ppm, Li^+ 975–1280 ppm (0.18 M LiCl), and B 1.440 ppm.

$LiMn_2O_4$/Pt electrodes were prepared by thermal decomposition of a $LiNO_3$ and $Mn(NO_3)_3$ mixed solution (Sigma Aldrich, Li: Mn molar ratio of 0.5) on a Pt sheet. The Pt substrate was coated with a thin layer of the solution which was first evaporated at 70 °C, further heated in air at 650 °C for 12 h and finally cooled down to room temperature, yielding a thin layer of polycrystalline single phase $LiMn_2O_4$ characterized by XRD and SEM.

The electrodes used in XRD experiments were prepared by casting a slurry of 80% w/w $LiMn_2O_4$ (Sigma Aldrich, battery grade), 10% PVDF (Sigma Aldrich) and 10% Carbon Vulcan X-72 (Cabot Corp.) suspended in N-methyl pyrrolidone (Sigma Aldrich) onto flat 1.3 cm^2 stainless steel plates and are labelled $LiMn_2O_4$/SS. The chloride reversible polypyrrole counter electrode was obtained by electrochemical polymerization of an aqueous solution of 0.1 M pyrrole/1.2 M HCl on large surface area platinum mesh (Goodfellow PT008710) under potential control at 1 V during 1 h. Aqueous solutions of natural brine, 0.1 M LiCl (Sigma Aldrich) and 0.1 M NaCl (Sigma Aldrich) were used as electrolytes.

Electrochemical experiments were carried out in a three-electrode undivided cell with a $LiMn_2O_4$ working electrode, a Polypyrrole/Pt counter electrode and an Ag/AgCl (in KCl 3 M) reference electrode (all potentials herein are quoted with respect to that reference), using an Autolab PGSTAT 30 potentiostat (Autolab, Ecochemie, Holland) equipped with Nova 1.10 software. Different states of charge were achieved by partial delithiation of $LiMn_2O_4$ (or partial lithiation of λ–MnO_2) by applying a constant potential until the current was well below 1 μA. In all cases, a meniscus was formed with the electrode surface touching the aqueous electrolyte solution. After the electrochemical treatment, the corresponding $Li_{1-x}Mn_2O_4$ ($0 \leq x \leq 1$) electrode was rinsed with MilliQ water, dried with constant flow of pure N_2 and finally examined ex situ using either X-ray photoelectron spectroscopy (XPS) or X-ray diffraction (XRD).

XPS measurements were performed within an ultrahigh vacuum chamber (UHV) with a base pressure below 5.10^{-10} mbar. The analysis chamber is equipped with a SPECS UHV spectrometer system which consists of a 150 mm mean radius hemispherical electron energy analyzer and a nine channeltron detector. XP spectra were acquired on grounded conducting substrates at a constant pass energy of 20 eV using a Mg Kα (1253.6 eV) source operated at 12.5 kV and 20 mA at a detection angle of 30° with respect to the sample normal. No charge compensation was necessary. Atomic ratios were calculated from the integrated intensities of core levels after instrumental and photoionization cross-section corrections. XPS spectra were fitted using CasaXPS processing software.

The x-ray diffraction patterns were obtained on a SIEMENS D5000 powder diffractometer, Cu-Kα radiation = 1.54056 Å. The spectra were recorded over a 2θ range from 15° to 90° with a step of 0.02° and a count time of 1 s/point.

3. Results and discussion

The morphology of the $LiMn_2O_4$ crystallites and their particle size distribution in the $LiMn_2O_4$/SS electrode was inspected by SEM.

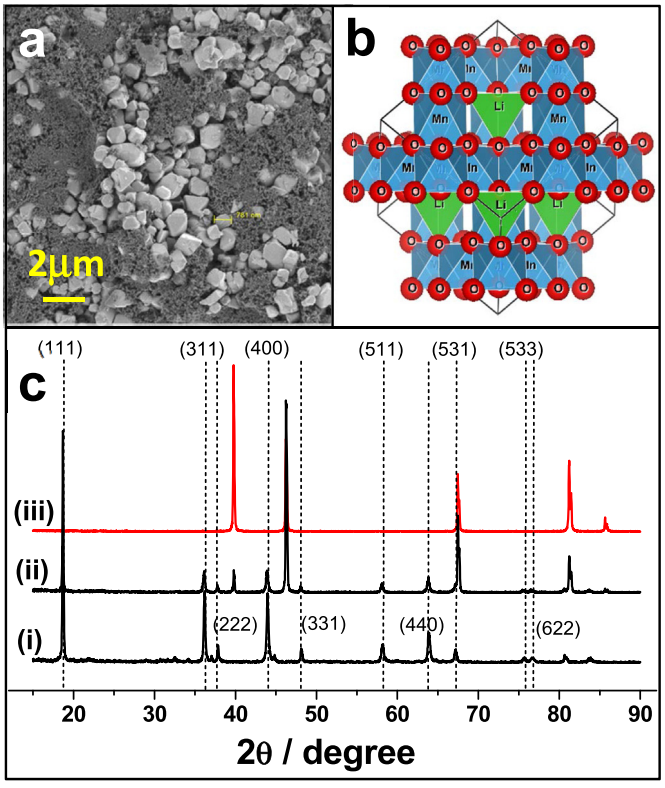

Fig. 1. (a) Scanning electron micrography of the stainless steel electrode casted with the $LiMn_2O_4$ slurry. (b) Polyhedral representation of spinel $LiMn_2O_4$ crystal structure. (c) X-ray diffractograms of (i) the stainless steel electrode cast with the $LiMn_2O_4$ slurry, (ii) the $LiMn_2O_4$/Pt electrode and (iii) a Pt sheet substrate.

Fig. 1a shows the SEM micrograph of a stainless steel electrode casted with the $LiMn_2O_4$ slurry. The particles corresponding to $LiMn_2O_4$ crystals are distributed in a carbon and PVDF darker background. Crystallites present an average size of 700 nm diameter and a size distribution going from 300 nm up to 1500 nm. The degree of crystallinity of the $LiMn_2O_4$ electrodes was examined by X-ray diffraction (XRD) measurements. Fig. 1c shows XRD diffraction patterns corresponding to (i) the $LiMn_2O_4$/SS electrode, (ii) the $LiMn_2O_4$/Pt electrode and (iii) a Pt sheet substrate. XRD peaks in diffraction patterns (i) and (ii) were indexed as a cubic spinel structure (F3dm space group) with a lattice parameter a = 8.24 Å obtained from the 2θ position of a (h k l) diffraction peak using the Bragg's law for a cubic phase: $a = \frac{\lambda \sqrt{h^2+k^2+l^2}}{2 \operatorname{sen} \theta}$.

The calculated lattice parameters from (511) reflection resulted, confirming the presence of a single crystalline phase without any observable residual impurities for the synthesized oxide. $LiMn_2O_4$ crystallizes in a stable spinel structure having the general formula $A[B_2]X_4$ which can be described as a cubic closed-packed framework of oxygen anions located in the 32e positions of the F3dm space group, with lithium cations occupying the 8a tetrahedral sites and Mn(III)/Mn(IV) cations in the 16d octahedral interstices, as shown in the polyhedral representation of the structure in Fig. 1b [30].

The surface chemical composition of the $LiMn_2O_4$/Pt electrode has been characterized by X-ray photoelectron spectroscopy (XPS). Manganese is often measured by XPS following the Mn 2p signal as it presents a higher sensitivity owing to its larger photoionization cross section. However Mn 2p is a complex signal with multiple splitting of the core lines and a small chemical shift as a function of the manganese oxidation state [31]. The manganese oxidation state in mixed valence oxides is also measured with XPS following the Mn 3s photoelectron signal. In this case, the core level line shows multiple splitting and the binding energy difference between the high- and low-spin components can be correlated to the relative content of Mn(III) ions. Notwithstanding, when different Mn(III)/Mn(IV) ratios are present a broadening of the low-spin component is observed, making it difficult to determine accurately the multiple splitting binding energy difference [32]. Therefore, it is more convenient to measure the changes in the manganese oxidation state following the Mn 3p core line [31]. Given that the binding energy position of the 3p peak changes with oxidation state and that the $3p_{3/2}$ and $3p_{1/2}$ doublet is not resolved then the Mn(III) and Mn(IV) components could each be fitted with a single peak [31].

Fig. 2a shows the XPS broad scan of a $LiMn_2O_4$/Pt electrode. The main signals are due to Li, Mn and O as expected, however we can also observe signals due to the Pt substrate and to a low content of adventitious C. Note that there is no evidence of Cl or Na on the surface. Fig. 2b shows the Mn 3p and Li 1s regions of the spectrum. In the spinel environment the Li 1s signal appears at 54 eV whereas Mn3p presents a broad peak centered at 49 eV. The low sensitivity factor for Li 1s (25 times smaller than the Mn 3p factor) hindered the determination of the lithium surface content in $Li_{1-x}Mn_2O_4$ cathodes at different values of x. As shown in Fig. 2b Li was only observed in the as prepared electrodes whose surfaces are lithium rich as it has been reported elsewhere [33]. As discussed above the Mn3p signal was fitted with two components corresponding to Mn(III) and Mn(IV) centered at 48.4eV and 50.3 eV respectively [31,33,34]. This resulted in a surface composition with 49% of Mn (III) and 51% of Mn(IV) in excellent agreement with the expected Mn(III):Mn(IV) 1:1 stoichiometry in $LiMn_2O_4$.

Lithium ions can be gradually inserted from brine into the $Li_{1-x}Mm_2O_4$ ($x \rightarrow 0$) spinel by applying a constant current or potential to form $Li_{1-x}Mn_2O_4$ ($0 < x \leq 1$). This process can be reversed extracting Li^+ ions from $Li_{1-x}Mn_2O_4$ into a LiCl recovery electrolyte by reversing the current. The lithiation process can be represented by the following reaction:

$$2\lambda\text{–}Mn^{IV}O_2 + x\,e^- + x\,Li^+ \rightarrow Li_xMn^{III}_xMn^{IV}_{(2-x)}O_4 \quad (0 < x \leq 1)$$

Further lithium insertion into $LiMn_2O_4$ is known to cause Jahn-Teller distortion due to the presence of unstable Mn(III) (electronic configuration d^4) in octahedral environments, which leads to an irreversible first order transition phase from cubic to tetragonal to form $Li_2Mn_2O_4$ by displacing the Li ions from the tetrahedral to the vacant 16c octahedral sites [3,35,36].

Fig. 3a shows a cyclic voltammetry (CV) of this oxide performed in natural brine containing 0.18 M LiCl and in 0.2 M LiCl at a scan rate of 2 mV/s using $LiMn_2O_4$/Pt electrodes. In agreement with the measurements obtained using organic electrolytes [3,6,36,37], the CV in aqueous media also exhibits two anodic peaks (at 0.90 V and 0.75 V) and their corresponding cathodic counterparts (0.71 V and 0.85 V), which are assigned to two stages in the Li^+ extraction/insertion processes [6]. Notice the smaller charge and shift towards higher potential in natural brine with respect to LiCl solution of similar Li^+ concentration. Fig. 4 shows that the integrated charge for surface the Mn^{IV}/Mn^{III} redox couple decreases as the NaCl concentration increases in LiCl + NaCl solutions with a minimum value for natural brine. This will be further discussed in terms of sodium adsorption and blocking of lithium adsorption sites as it resulted from kinetic measurements [29]. The shift to higher potentials is due to the activity of LiCl in natural brine.

Fig. 3b exhibits the evolution of potential during one cycle of Li^+

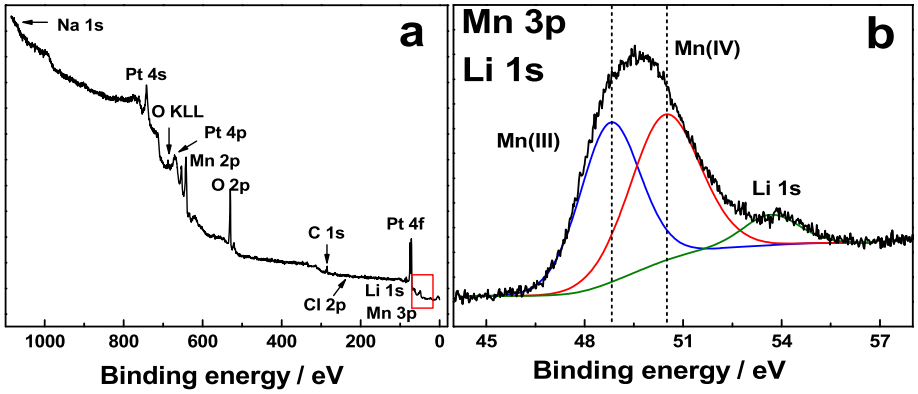

Fig. 2. XPS analysis on the as prepared $LiMn_2O_4$/Pt electrode. (a) XPS broad scan exhibiting the expected signals and a small signal from adventitious C. (b) Mn 3p and Li 1s XPS signals. Mn 3p has been fitted with two components due to Mn(III) (blue) and Mn(IV) (red). (For interpretation of the references to colour in this figure legend, the reader is referred to the Web version of this article.)

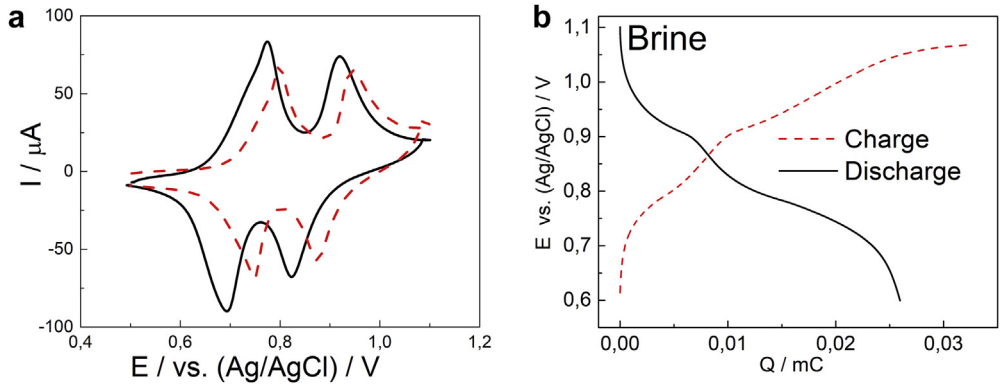

Fig. 3. (a) Cyclic voltammetry of $LiMn_2O_4$/Pt electrode in 0.1 M LiCl (black) and natural brine (red) at a scan rate of 2 mV s^{-1}. (b) Galvanostatic charge (red) and discharge (black) curves of a $LiMn_2O_4$/Pt electrode in natural brine at a constant current density of ±50 μA/cm^2 in natural brine. The areal loading obtained by weight difference was typically 15 mg cm^{-2}. (For interpretation of the references to colour in this figure legend, the reader is referred to the Web version of this article.)

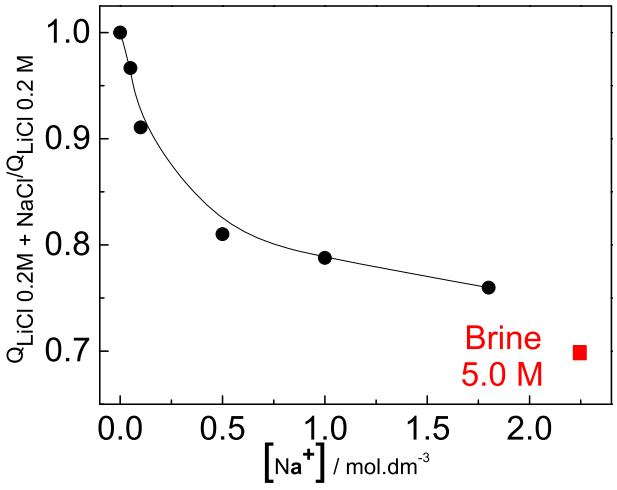

Fig. 4. Normalized voltammetry charge to the charge in the absence of sodium ions in the electrolyte vs. concentration of sodium in the LiCl + NaCl electrolyte.

extraction/insertion (black/red curve, respectively) of $Li_{1-x}Mn_2O_4$ in brine at a constant current of ±500 μA. As expected the charge corresponding to the extraction and the charge corresponding to the insertion, depends on the initial state of charge. Furthermore, the galvanostatic curves of charge and discharge of $Li_{1-x}Mn_2O_4$ show two plateaux in the $0.95 < x < 0.63$ and $0.41 < x < 0.19$ composition ranges. Topotactic lithium extraction from $Li_{1-x}Mn_2O_4$ (or insertion into λ-MnO_2 i.e. $x \rightarrow 0$) takes place with isotropic shrinkage (or expansion) of the crystal lattice retaining the original cubic symmetry. Nevertheless, while extracting or inserting Li^+, the crystal structure undergoes several phase transitions between different cubic structures depending on the lithium content [38]. In-situ X-ray studies demonstrated that two phase transitions occur between three cubic phases [39]. One phase is present at $x = 1$ while two phases coexist in the range $0.65 < x < 1$. The second phase is unique for $0.55 < x < 0.65$, while a third phase emerges and coexists with the second phase in the range of $0.27 < x < 0.55$. The third phase at the end of lithium extraction corresponds to the fully delithiated $Li_{1-x}Mn_2O_4$ ($x \rightarrow 0$) crystal structure. When homogeneous lithium extraction takes place, a change in the free energy of the solid should be observed causing the electrode potential to vary. On the other hand, when two different phases coexist, the potential is expected to remain constant as the composition changes giving a flat voltage plateau in the charge/discharge galvanostatic curves [40]. In Fig. 3b two stages are observed for composition ranges $0.95 < x < 0.63$ and $0.41 < x < 0.19$ with sloped plateaux due to non-ideality in the solid solution which arise form interactions.

Structural changes due to topotactic lithium extraction/insertion from/into $Li_{1-x}Mn_2O_4$ ($0 \leq x \leq 1$) crystal lattice are evidenced as a shift in XRD peaks due to the contraction/expansion of the unit cell. Fig. 5a shows the ex-situ XRD diffraction pattern in the 2θ region from 57° to 61° (Cu-Kα) corresponding to the (511) diffraction peak. Peaks a, b and c correspond to a $Li_{1-x}Mn_2O_4$ electrode with compositions $x = 1$, $x = 0.5$ and $x \rightarrow 0$ respectively. The Li composition was modified after 1 h polarization in 0.1 M LiCl (Fig. 5a) or natural brine (Fig. 5b) at different potentials (0.6 V for peak a, 0.85 V for peak b and 1.1 V for peak c). As expected, the higher the lithium content in the spinel, the more shifted the peak towards higher 2θ values the peak is, confirming the insertion of Li^+ ions within the bulk structure of the oxide. We can calculate the $LiMn_2O_4$ unit cell lattice parameter from the 2θ position of the (511) diffraction peak. The calculated lattice parameters are 8.24 Å for the fully lithiated structure ($x = 1$), 8.16 Å for the spinel with half lithium content ($x = 0.5$) and 8.04 Å for the $Li_{1-x}Mm_2O_4$ ($x \rightarrow 0$) phase. These values are in close agreement with the reported values for the three cubic phases observed in $Li_{1-x}Mn_2O_4$ electrodes in organic electrolytes [13,39]. The lattice parameter cannot be varied continuously as the Li content is modified, instead the spinel crystal undergoes two first order cubic phase transitions during charge and discharge. Therefore, the determined lattice parameters can be assigned to the three different cubic phases [41].

Lithium rich natural brines have a Li content up to 25 times smaller than the sodium content. Therefore, the possibility of Na^+ ion insertion into the oxide structure must be considered. We have attempted to insert Na^+ by polarizing a fully delithiated $Li_{1-x}Mm_2O_4$ ($x \rightarrow 0$) electrode at 0.6 V for 1 h in a 0.1 M NaCl electrolyte. The resulting XRD measurement is shown in Fig. 5 (peak d). The position of the (511) diffraction peak does not exhibit any change with respect to the peak due to the lithium free spinel (peak c). Clearly, no structural changes take place after cathodic polarization in a NaCl solution and therefore no Na^+ insertion into the crystal occurred at the potential of Li^+ insertion.

The lack of Na^+ insertion into the spinel crystal was also observed electrochemically. Fig. 6 shows CVs of a fresh $LiMn_2O_4$ cycled in a NaCl 1 M solution. The two typical anodic peaks are only observed during the first cycle, indicating Mn(III) oxidation to Mn(IV) and the consequent lithium leach from the crystal lattice. In cycle 2 the anodic peaks decrease in intensity and shift towards lower potentials, whereas in cycle 3 they completely disappear. Most of the lithium content of the spinel that was extracted during

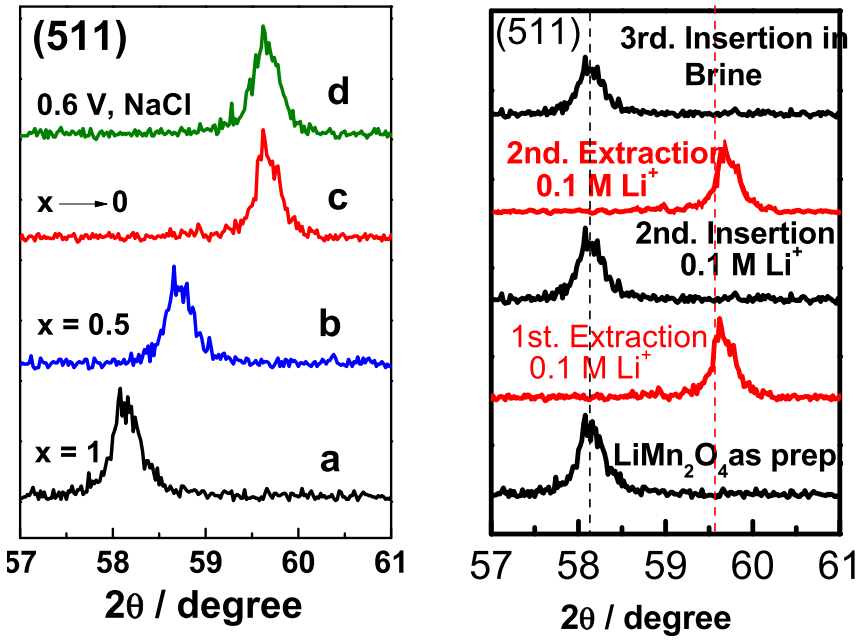

Fig. 5. X-ray diffraction patterns of a stainless steel electrode cast with the $Li_xMn_2O_4$ slurry in the 2θ region from 57° to 61° (Cu-Kα), where (511) peak appears. Peaks indicated as (a), (b) and (c) correspond to different states of charge represented with the *x* value and reached after 1 h polarization at different potentials: 0.6 V for peak (a), 0.85 V for peak (b) and 1.1 V for peak (c), in LiCl 0.1 M. Peak (d) corresponds to the resulting pattern after 1 h polarization of the delithiated structure of peak (c) at 0.6 V in 0.1 M NaCl. Right top: Lithium insertion from natural brine.

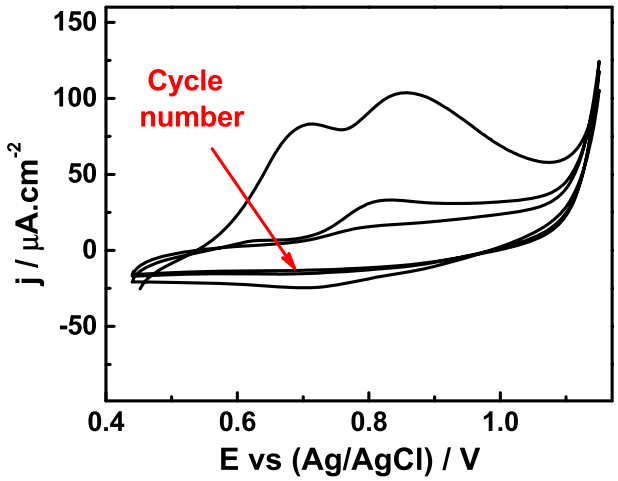

Fig. 6. Cyclic voltammetry (3 cycles) of a $LiMn_2O_4$/Pt electrode in a 1 M NaCl solution at a scan rate of 2 mV s^{-1}.

the first cycle diffused into the solution far from the electrode and cannot be reinserted back due to a very low concentration. But a small fraction of the lithium extracted in the first cycle remained in the double layer and was reinserted within the crystal in the following cycle, yielding one small cathodic peak around 0.70 V, which disappears in the subsequent potential sweeps. Since the Na^+ ions in solution cannot be inserted in the crystal structure as we have shown above no redox activity for Mn ions in the oxide is observed after cycle 2 resulting in a flat CV.

Li^+ insertion into the crystal is accompanied by the reduction of Mn(IV) to Mn(III) which could be reflected on the surface composition of the spinel. Therefore, we have performed XPS measurements to determine the Mn(III) and Mn(IV) surface composition as a function of Li composition in the $Li_{1-x}Mn_2O_4$ crystal. Fig. 7a shows the Mn 3p XPS spectra of $LixMn_2O_4$/Pt electrodes after 1 h polarization at different potentials in 0.1 M LiCl solutions. Specifically, polarization was carried out at 0.6 V (fully discharged), 0.75 V, 0.85 V and 1.1 V (fully charged) which correspond to $x = 1$, 0.7, 0.4 and 0 respectively. Initially the electrode was fully discharged ($x = 1$) and the surface contained around 49% Mn(III). Subsequent electrochemical lithium extraction obtained by increasing the electrode potential resulted in a continuous decrease in the Mn(III) component of Mn3p XPS signal until it complete vanishes when the electrode is fully charged ($x = 0$). At this point all Mn(III) is oxidized to Mn(IV). Complementary the Mn(IV) component increases linearly with electrode potential during the charge process as shown in Fig. 7b. The above results show that the Mn(III):Mn(IV) surface composition can be controlled with the electrode potential and that there is no preferential surface segregation of any of the oxidation states of Mn. We should note that the $Li_{1-x}Mn_2O_4$ electrode surface composition was retained after opening the circuit once the electrochemical treatment was finished and removing the electrode from the aqueous electrolyte for ex-situ measurements in UHV.

The exposure of surface Mn(III) to aqueous solutions represents a potential problem. When non-aqueous electrolytes are employed a surface layer of decomposition products is formed. These passivation films are an essential component for the successful cycling of Li-ion batteries as they are a good Li^+ ion conductor which prevents surface Mn(III) from getting in contact with the electrolyte avoiding dismutation into Mn(IV) and soluble Mn(II) [42]. However, our XPS measurements indicate that no surface layer is formed when cycling $LiMn_2O_4$ in aqueous media. Thus, Mn(III) rich surfaces in contact with an aqueous electrolyte could result in the unwanted loss of Mn. We have therefore discharged and charged $LiMn_2O_4$ in aqueous solutions 55 times in 72 h and found that only 0.17% of the initial Mn in the electrode is lost to the solution. This result is in good agreement with the loss of capacity with the number of cycles shown in Fig. 8. The electrode losses 15% of the initial capacity in the first 20 cycles and then the capacity remains approximately constant. This is, capacity fading is not due

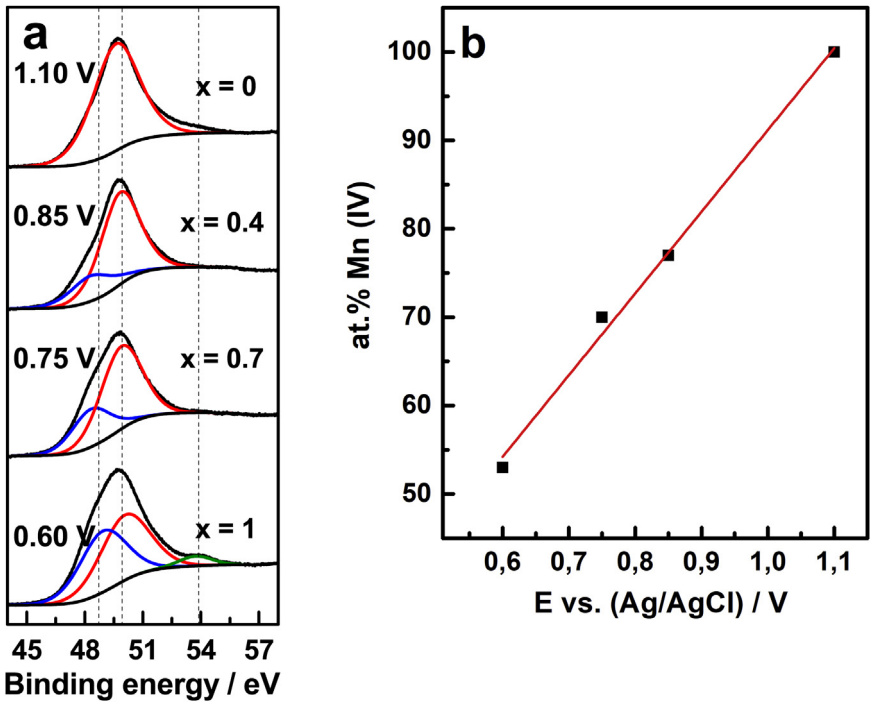

Fig. 7. (a) Mn 3p XPS signals of a $LiMn_2O_4$/Pt electrode at different states of charge represented with the *x* value and reached after 1 h polarization at the indicated potentials in 0.1 M LiCl. Mn 3p has been fitted with two components corresponding to Mn(III) (blue) and Mn(IV) (red). (b) Surface Mn (IV) percent vs. applied potential. (For interpretation of the references to colour in this figure legend, the reader is referred to the Web version of this article.)

to the very small loss of Mn into the solution and could be due to changes in the morphology of the film that modifies the electroactive area.

We have shown above that Na^+ ions are not inserted into the bulk structure of $Li_{1-x}Mn_2O_4$ however they could still adsorb on the electrode surface blocking Li adsorption surface tetrahedral sites. The integrated charge in the cyclic voltammetry (Fig. 4) decreases with the increase in NaCl concentration. Fig. 9a and b shows Mn 3p and Na 1s XPS spectra of a $Li_{1-x}Mn_2O_4$ electrode surface before and after 1 h polarization in a 0.1 M NaCl electrolyte at 0.6 V. Initially, the fully delithiated electrode contains only Mn(IV) and has no sodium adsorbed. After the electrochemical treatment Na is adsorbed on the surface. Here we should note that no chloride anions are observed on the surface, thus ruling out a non-properly rinsed electrode surface as the source of sodium cations.

Furthermore, the appearance of sodium cations on the surface is accompanied by the appearance of Mn (III) due to the electrochemical reduction of the surface due to the applied potential. Therefore, we conclude that Na^+ ions at the surface compensate the positive charge in the surface Mn(IV) to Mn(III) reduction.

The above results indicate that Na^+ ions could compete with Li^+ ions for surface adsorption sites and this could also decrease the rate of lithium intercalation in LiCl solutions. Fig. 10 shows CVs of a $LiMn_2O_4$ electrode in a 0.1 M LiCl electrolyte carried out before (dash line) and after (full line) cycling the electrode in a 0.1 M NaCl electrolyte. The charge calculated from the CV integrated current after cycling in 0.1 M NaCl dropped by 50% with respect to the initial charge. Here we should note that the initial charge could not be recovered even after 10 cycles in 0.1 M LiCl. These results could be rationalized as discussed above, sodium cations irreversibly block lithium adsorption sites lowering the rate of Li^+ intercalation. Furthermore, peak separation for both the anodic and cathodic peak pairs increased also in line with slower kinetics. This agrees with our recent electrochemical impedance spectroscopy results which show that the charge transfer resistance increases with increasing the NaCl concentration in the electrolyte [29].

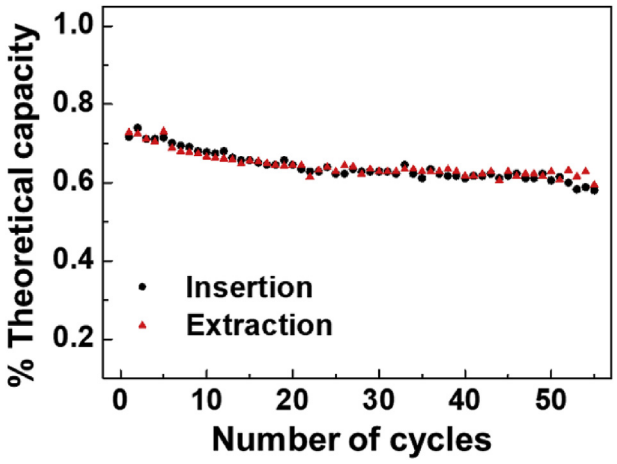

Fig. 8. Capacity fading of $Li_xMn_2O_4$/SS electrode cycled in 0.1 M LiCl between 0.5 V and 1.05 V at a constant current of +500 μA.

4. Conclusions

Li^+ ions in aqueous solution can be reversibly inserted/extracted into/from $Li_{1-x}Mn_2O_4$ ($0 \leq x \leq 1$) electrodes upon the application of suitable electrode potential. The insertion/extraction of Li^+ from natural brine or LiCl solutions proceeds via a two stage process and the cubic spinel undergoes two reversible phase transitions as the lattice is contracted/expanded. In agreement with the behavior in organic electrolytes three cubic phases with 8.24 Å, 8.16 Å and 8.04 Å lattice parameters are observed. Contrary to the behavior in

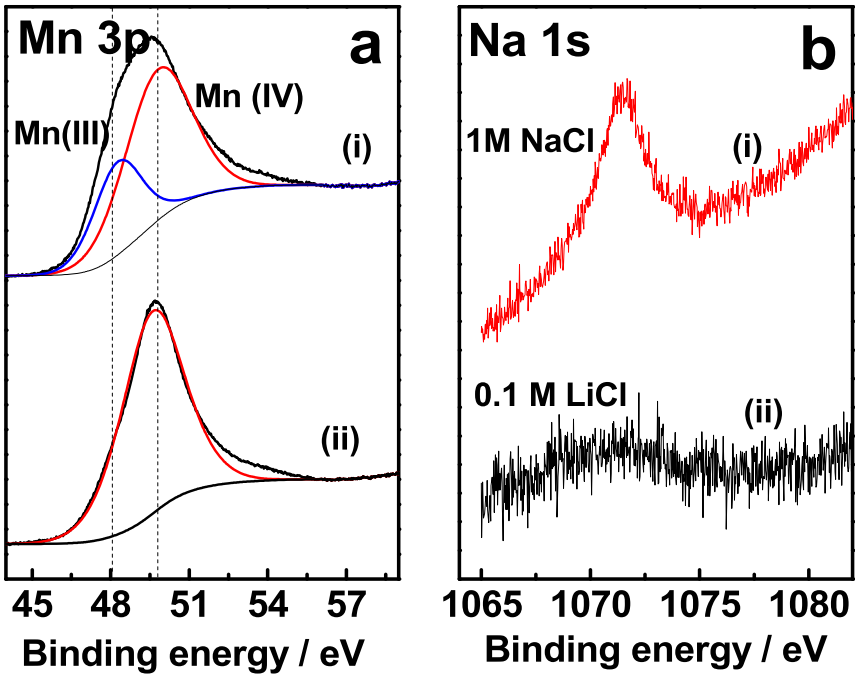

Fig. 9. (a) Mn 3p and (b) Na 1s XPS signals of an initially fully delithiated λ-Mn_2O_4/Pt electrode (i) before and (ii) after 1 h polarization at 0.6 V in 0.1 M NaCl. No evidence of chloride anions on the surface was found.

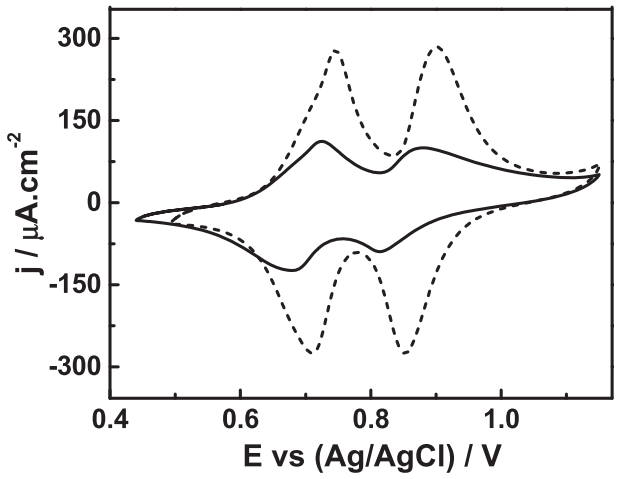

Fig. 10. Cyclic voltammetry of a $LiMn_2O_4$/Pt electrode in 0.1 M LiCl at a scan rate of 2 mV s^{-1} after cycling in 0.1M NaCl (solid line) or in the absence of sodium (dashed line).

organic electrolytes, no surface decomposition layer is formed. The electrode potential controls the surface Mn(III):Mn(IV) composition. There is no preferential surface segregation of one particular Mn oxidation state instead the Mn(IV) concentration increases linearly with electrode potential (Li^+ extraction). Electrochemical polarization in the presence of Na^+ in solution does not result in the insertion of Na^+ into the crystal structure. However, Na^+ adsorbs at the electrode surface blocking Li^+ adsorption sites and thus lowering the rate of Li^+ insertion into the lattice. Repetitive insertion/extraction cycles resulted in the small loss of Mn into the electrolyte solution (0.17% after 72 h). Therefore, practical use of $LiMn_2O_4$ to extract Li^+ from seawater or natural brines would require addressing this small loss of Mn upon cycling.

Acknowledgements

Funding from University of Buenos Aires and CONICET and ANPCyT PICT 2014 No. 3654 and a research doctoral fellowship from CONICET to F.M. are gratefully acknowledged.

References

[1] M.S. Whittingham, Lithium batteries and cathode materials, Chem. Rev. 104 (2004) 4271–4301.
[2] E.V. Makhonina, V.S. Pervov, V.S. Dubasova, Oxide materials as positive electrodes of lithium-ion batteries, Russ. Chem. Rev. 73 (2007) 991–1001.
[3] M.M. Thackeray, P.J. Johnson, L.A. de Picciotto, P.G. Bruce, J.B. Goodenough, Electrochemical extraction of lithium from LiMn2O4, Mater. Res. Bull. 19 (2) (1984) 179–187.
[4] M.M. Thackeray, W.I.F. David, P.G. Bruce, J.B. Goodenough, Lithium insertion into manganese spinels, Mater. Res. Bull. 18 (1983) 461–472.
[5] J.M. Tarascon, Li metal-free rechargeable batteries based on Li(1+x)Mn2O4 cathodes ($0 \leq x \leq 1$) and carbon anodes, J. Electrochem. Soc. 138 (1991) 2864.
[6] M. Rossouw, A. de Kock, L. de Picciotto, M. Thackeray, W. David, R. Ibberson, Structural aspects of lithium-manganese-oxide electrodes for rechargeable lithium batteries, Mater. Res. Bull. 25 (1990) 173–182.
[7] K. Ooi, Y. Miyai, S. Katoh, H. Maeda, M. Abe, Topotactic Li+ insertion to λLi1-XMm2O4 (x → 0)in the aqueous phase, Langmuir 5 (1989) 150–157.
[8] H. Kanoh, K. Ooi, Y. Miyai, S. Katoh, Selective electroinsertion of lithium ions into a Pt/λLi1-XMm2O4 (x → 0)electrode in the aqueous phase, Langmuir 7 (1991) 1841–1842.
[9] S. Mishra, G. Ceder, Structural stability of lithium manganese oxides, Phys. Rev. B 59 (1999) 6120–6130.
[10] H. Berg, K. Go, B. Nola, J.O. Thomas, Electronic Structure and Stability of the Li, vol. 4, 1999, pp. 2813–2820.
[11] J. Dong H, Y.J. Shin, S.M. Oh, Dissolution of spinel oxides and capacily losses in 4 V, J. Electrochem. Soc. 143 (1996) 2204–2211.
[12] P. Arora, Capacity fade mechanisms and side reactions in lithium-ion batteries, J. Electrochem. Soc. 145 (1998) 3647.
[13] Y. Xia, M. Yoshio, An investigation of lithium ion insertion into spinel structure Li-Mn-O compounds, J. Electrochem. Soc. 143 (1996) 825.
[14] T. Hoshino, Development of technology for recovering lithium from seawater by electrodialysis using ionic liquid membrane, Fusion Eng. Des. 88 (2013) 2956–2959.
[15] N. Intaranont, N. Garcia-Araez, A.L. Hector, J.A. Milton, J.R. Owen, Selective lithium extraction from brines by chemical reaction with battery materials, J. Mater. Chem. A 2 (2014) 6374–6377.
[16] J. Lee, S.-H. Yu, C. Kim, Y.-E. Sung, J. Yoon, Highly selective lithium recovery from brine using a λ-MnO2–Ag battery, Phys. Chem. Chem. Phys. 15 (2013)

7690.
[17] R. Trocoli, G.K. Bidhendi, F. La Mantia, Lithium recovery by means of electrochemical ion pumping: a comparison between salt capturing and selective exchange, J. Phys. Condens. Matter 28 (2016) 114005.
[18] H. Kanoh, K. Ooi, Y. Miyai, S. Katoh, Electrochemical recovery of lithium ions in the aqueous phase, Separ. Sci. Technol. 28 (1993) 643–651.
[19] R. Trócoli, A. Battistel, F. La Mantia, Selectivity of a lithium-recovery process based on LiFePO 4, Chem. A Eur J. 20 (2014) 9888–9891.
[20] H. Kanoh, AC impedance analysis for Li+ insertion of a Pt/λLi1-XMm2O4 (x 0) Electrode in an aqueous phase, J. Electrochem. Soc. 143 (1996) 2610.
[21] D. Aurbach, K. Gamolsky, B. Markovsky, G. Salitra, Y. Gofer, U. Heider, R. Oesten, M. Schmidt, The study of surface phenomena related to electrochemical lithium intercalation into LixMOy host materials (M = Ni, Mn), J. Electrochem. Soc. 147 (2000) 1322.
[22] K. Edström, T. Gustafsson, J.O. Thomas, The cathode-electrolyte interface in the Li-ion battery, Electrochim. Acta 50 (2004) 397–403.
[23] L.L. Missoni, F. Marchini, M. del Pozo, E.J. Calvo, A LiMn2O4 -polypyrrole system for the extraction of LiCl from natural brine, J. Electrochem. Soc. 163 (2016) A1898–A1902.
[24] F. Marchini, E.J. Calvo, Method and Electrochemial Device for Low Environmental Impact Lithium Reovery from Aqueous Solutions, US 2014/0076734 A1, 2014.
[25] J.P. Parant, R. Olazcuaga, M. Devalette, C. Fouassier, P. Hagenmuller, Sur quelques nouvelles phases de formule NaxMnO2 (x ≤ 1), J. Solid State Chem. 3 (1971) 1–11.
[26] J.M. Tarascon, D.G. Guyomard, B. Wilkens, W.R. Mc Kinnon, P. Barboux, Chemical and electrochemical insertion of Na into the spinel λLi1-XMm2O4 (x 0)phase, Solid State Ionics 57 (1992) 113–120.
[27] D. Tang, L. Ben, Y. Sun, B. Chen, Z. Yang, L. Gu, X. Huang, Electrochemical behavior and surface structural change of LiMn $_2$ O $_4$ charged to 5.1 V, J. Mater. Chem. A 2 (2014) 14519–14527.
[28] F. Marchini, D. Rubi, M. Del Pozo, F.J. Williams, E.J. Calvo, Surface chemistry and lithium-ion exchange in LiMn2O4 for the electrochemical selective extraction of LiCl from natural salt lake brines, J. Phys. Chem. C 120 (2016).
[29] F. Marchini, F.J. Williams, E.J. Calvo, Electrochemical impedance spectroscopy study of the Li_1-xMn2O4 interface with natural brine, Electroanal. Chem. (2017), https://doi.org/10.1016/j.jelechem.2017.11.071 (In press).
[30] H. Björk, T. Gustafsson, J.O. Thomas, S. Lidin, V. Petříček, Long-range ordering during delithiation of LiMn2O4 cathode material, J. Mater. Chem. 13 (2003) 585–589.
[31] J.M. Cerrato, M.F. Hochella, W.R. Knocke, A.M. Dietrich, T.F. Cromer, Use of XPS to identify the oxidation state of Mn in solid surfaces of filtration media oxide samples from drinking water treatment plants, Environ. Sci. Technol. 44 (2010) 5881–5886.
[32] A.G. Kochur, A.T. Kozakov, A.V. Nikolskii, K.A. Googlev, A.V. Pavlenko, I.A. Verbenko, L.A. Reznichenko, T.I. Krasnenko, Valence state of the manganese ions in mixed-valence La1−αBiβMn1+δO3±γ ceramics by Mn 2p and Mn 3s X-ray photoelectron spectra, J. Electron. Spectrosc. Relat. Phenom. 185 (2012) 175–183.
[33] T. Eriksson, A.M. Andersson, A.G. Bishop, C. Gejke, T. Gustafsson, J.O. Thomas, Surface analysis of LiMn2O4 electrodes in carbonate-based electrolytes, J. Electrochem. Soc. 149 (2002) A69.
[34] M. Oku, K. Hirokawa, S. Ikeda, X-ray photoelectron spectroscopy of manganese-oxygen systems, J. Electron. Spectrosc. Relat. Phenom. 7 (1975) 465–473.
[35] W.I.F. David, M.M. Thackeray, L.A. De Picciotto, J.B. Goodenough, Structure refinement of the spinel-related phases Li2Mn2O4 and Li0.2Mn2O4, J. Solid State Chem. 67 (1987) 316–323.
[36] E.C.A. Rougier, K.A. Striebel, S.J. Wen, Cyclic voltammetry of pulsed laser deposited LixMn2O4 thin films, J. Electrochem. Soc. 145 (1998) 2975.
[37] F.K. Shokoohi, Low temperature LiMn2O4 spinel films for secondary lithium batteries, J. Electrochem. Soc. 139 (1992) 1845.
[38] T. Ohzuku, M. Kitagawa, T. Hirai, Electrochemistry of manganese dioxide in lithium nonaqueous cell, J. Electrochem. Soc. 137 (1990) 769.
[39] X.Q. Yang, X. Sun, S.J. Lee, J. McBreen, S. Mukerjee, M.L. Daroux, X.K. Xing, In situ synchrotron X-ray diffraction studies of the phase transitions in LixMn2O4 cathode materials, Electrochem. Solid State Lett. 2 (1999) 157.
[40] K. Kanamura, H. Naito, T. Yao, Z. Takehara, Structural change of the LiMn2O4 spinel structure induced by extraction of lithium, J. Mater. Chem. 6 (1996) 33.
[41] H. Björk, T. Gustafsson, J.O. Thomas, Single-crystal studies of electrochemically delithiated LiMn2O4, Electrochem. Commun. 3 (2001) 187–190.
[42] J.C. Hunter, Preparation of a new crystal form of manganese dioxide: λ-MnO2, J. Solid State Chem. 39 (1981) 142–147.